Chaos
An Interdisciplinary Journal of Nonlinear Science

RESEARCH ARTICLE | OCTOBER 01 2025

Control of chimera states via adaptive higher-order interactions

Andrey V. Andreev ; Artem A. Badarin ; Dibakar Ghosh ; Elena N. Pitsik ; Alexander E. Hramov

Check for updates

Chaos 35, 101102 (2025)
https://doi.org/10.1063/5.0296464

View Online
Export Citation

Articles You May Be Interested In

Mixed-mode chimera states in pendula networks

Chaos (October 2022)

Is repulsion good for the health of chimeras?

Chaos (October 2017)

Effect of higher-order interactions on chimera states in two populations of Kuramoto oscillators

Chaos (February 2024)

06 October 2025 08:30:41

AIP Publishing

AIP Publishing
Chaos
Special Topics Open for Submissions
Learn More

Chaos ARTICLE pubs.aip.org/aip/cha

Control of chimera states via adaptive higher-order interactions

Cite as: Chaos **35**, 101102 (2025); doi: 10.1063/5.0296464
Submitted: 13 August 2025 · Accepted: 18 September 2025 ·
Published Online: 1 October 2025

View Online Export Citation CrossMark

Andrey V. Andreev,[1,2,a)] Artem A. Badarin,[1,2] Dibakar Ghosh,[3] Elena N. Pitsik,[1] and Alexander E. Hramov[1,2]

AFFILIATIONS

[1]Baltic Center for Neurotechnology and Artificial Intelligence, Immanuel Kant Baltic Federal University, 236041 Kaliningrad, Russia
[2]Research Institute of Applied Artificial Intelligence and Digital Solutions, Plekhanov Russian University of Economics, 115054 Moscow, Russia
[3]Physics and Applied Mathematics Unit, Indian Statistical Institute, 203 B. T. Road, Kolkata 700108, India

[a)]**Author to whom correspondence should be addressed:** andreevandrei1993@gmail.com

ABSTRACT

In recent years, adaptive higher-order interactions have garnered significant attention. However, most studies on chimera states in higher-order interaction networks have not considered coupling adaptation. In this work, we study a network of Kuramoto phase oscillators with first- and second-order interactions and adaptive couplings in two different network topologies: nonlocal and small-world. We show that, depending on the coupling strength, adaptation can induce a chimera state (where part of the network is synchronized, while the rest remains asynchronous) from a synchronous state or, conversely, synchronize a chimera state. Additionally, we find that small-world networks of Kuramoto phase oscillators exhibit a larger region of chimera states compared to nonlocal networks. Randomness of the topology realization plays an important role, and averaging over a number of realizations leads to increasing the possibility of a chimera state establishing. This work presents a novel approach to controlling the dynamics of adaptive higher-order interaction networks.

Published under an exclusive license by AIP Publishing. https://doi.org/10.1063/5.0296464

06 October 2025 08:30:41

Chimera states, characterized by the coexistence of synchronized and desynchronized dynamics within a network of coupled oscillators, represent a fascinating phenomenon in nonlinear science. In this work, we explore how adaptive higher-order interactions influence the emergence and stability of chimera states in networks of Kuramoto phase oscillators. By introducing dynamic adaptation mechanisms for both first-order (pairwise) and second-order (non-pairwise) coupling strengths, we uncover a rich spectrum of dynamical transitions. Our results demonstrate that coupling adaptation can actively control network behavior, inducing chimera states from fully synchronized regimes or, conversely, synchronizing previously disordered states. We systematically compare two fundamental network topologies, nonlocal and small-world, revealing that small-world architectures support a significantly broader parameter range for chimera states. Furthermore, the inherent randomness in small-world topology realizations enhances the robustness of these states, as confirmed by ensemble averaging. Notably, adaptive coupling enables the formation of antiphase synchronized clusters from incoherent dynamics or the destabilization of synchronization into chimera patterns. These findings are rigorously quantified using the strength of incoherence measure and spatiotemporal analysis.

I. INTRODUCTION

The study of synchronization in complex networks has been a central topic in nonlinear dynamics and complex systems theory for decades. Synchronization phenomena are observed in a wide range of natural and artificial systems, from biological neural networks to power grids and coupled oscillators.[1–5] Among the most widely studied models for understanding synchronization is the Kuramoto model, which describes the dynamics of coupled phase oscillators and has become a paradigmatic framework for exploring collective behavior in networks.[6–11]

In recent years, there has been growing interest in the role of higher-order interactions in shaping the dynamics of complex

Published under an exclusive license by AIP Publishing

systems.[12–15] Traditional models of network dynamics often focus on pairwise interactions, but many real-world systems exhibit interactions that involve three or more units simultaneously. These higher-order interactions can significantly influence the collective behavior of networks, leading to phenomena, such as multistability, first-order transition, cluster synchronization, and the emergence of chimera states.[14–20] Chimera states, characterized by the coexistence of synchronous and asynchronous dynamics within the same network, have attracted particular attention due to their counterintuitive nature and potential applications in neuroscience and other fields.[21–26]

Higher-order interactions, which go beyond the traditional pairwise connections, are increasingly recognized as essential for understanding the behavior of complex systems. For instance, in social networks, group interactions (e.g., team collaborations or group decision-making) often involve more than two individuals and cannot be fully captured by pairwise relationships.[27] Similarly, in biological systems, such as neural networks, interactions among multiple neurons (e.g., through synaptic triads or glial cells) play a crucial role in information processing and network dynamics. These higher-order interactions can lead to new types of collective behavior that are not observed in systems with only pairwise connections, such as the stabilization of specific synchronization patterns or the emergence of novel dynamical states.[28]

The adaptation of coupling strengths in dynamical networks is another important factor that can profoundly affect synchronization patterns.[29] Adaptive networks, where the coupling strengths evolve over time based on the system's dynamics, provide a more realistic representation of many biological and technological systems. For example, in neural networks, synaptic plasticity allows for the adaptation of connections between neurons, which is crucial for learning and memory processes.[30] The previous studies[18,21] on higher-order interactions inducing chimera states were observed without any adaptation in the coupling functions. Understanding how adaptive mechanisms influence synchronization in networks with higher-order interactions is, therefore, of great theoretical and practical importance.

In this work, we numerically investigate a network of Kuramoto phase oscillators with first- and second-order interactions, where the coupling strengths adapt over time. We consider two network topologies: a nonlocal topology and a small-world topology, which are known to exhibit distinct synchronization properties. Our goal is to explore how the adaptation of couplings influences the emergence and stability of different synchronization regimes, including synchronous, asynchronous, and chimera states. By analyzing the interplay between higher-order interactions and adaptive coupling mechanisms, we aim to provide new insights into the control and manipulation of synchronization patterns in complex networks.

The rest of the paper is organized as follows. In Sec. II, we describe the model of Kuramoto oscillators with higher-order interactions and adaptive couplings, as well as the methods used to quantify synchronization and classify different regimes. In Sec. III, we present the results of our numerical simulations for both nonlocal and small-world topologies, highlighting the effects of coupling adaptation on the network dynamics. Finally, in Sec. IV, we summarize our findings and discuss their implications for the study of complex systems.

II. METHODS

A. Adaptive higher-order interaction network

We consider a network of N Kuramoto phase oscillators with higher-order interactions and adaptation of couplings described by the following system of differential equations:

$$\frac{d\varphi_i}{dt} = \omega + L_1 \sum_{j=1}^{N} C_{ij}^1 \sin(\varphi_j - \varphi_i) + L_2 \sum_{j=1}^{N}\sum_{k=1}^{N} C_{ijk}^2 \sin(\varphi_j + \varphi_k - 2\varphi_i), \tag{1}$$

where φ_i is the phase of the ith oscillator ($i = 1, 2, \ldots, N$), $\omega = 1$ is the frequency of oscillators, and L_1 and L_2 are the strengths of the couplings of the pairwise (first order) and non-pairwise (second order) interactions, respectively. Here, C^1 and C^2 are the adjacency matrix and tensor of the pairwise and non-pairwise couplings, respectively. The elements of C^1 and C^2 are adapted as follows:

$$\begin{aligned} \frac{dC_{ij}^1}{dt} &= \rho_1 \left(R - C_{ij}^1\right), \\ \frac{dC_{ijk}^2}{dt} &= \rho_2 \left(R - C_{ijk}^2\right), \end{aligned} \tag{2}$$

where $\rho_{1,2}$ are the speeds of the adaptations and R is the global order parameter described as

$$R = \frac{1}{NT_m} \sum_{\tau=1}^{T_m} \left| \sum_{i=1}^{N} e^{\sqrt{-1}\varphi_i(t-\tau)} \right|, \tag{3}$$

where $T_m = 100$.

Initial coupling matrix C^0 is randomly generated using the Watts–Strogatz algorithm[31] with parameters k (node degree) and p (rewiring probability). We consider two network topologies: (i) a nonlocal one with $k = 4$ and $p = 0$ and (ii) a "small world" with $k = 5$ and $p = 0.3$. This matrix is used as the initial pairwise connectivity; i.e., $C^1 = C^0$. The second-order interaction tensor C^2 is then constructed by identifying all-to-all connected triangles within this network. During a transient period $t < T_a = 40$, the adaptation is turned off, so $\dot{C}_{ij}^1 = \dot{C}_{ijk}^2 = 0$. For $t \geq T_a$, $\dot{C}_{ij}^1$ and $\dot{C}_{ijk}^2$ are calculated using Eq. (2).

The system of differential equations (1) and (2) is solved by using 4th order Runge–Kutta methods with time step $\Delta t = 0.01$ and $N = 100$. The initial conditions of φ_i are generated randomly in a uniform distribution $[0, 2\pi]$ and used for all simulations.

B. Measure of synchronization

In order to properly distinguish the three different parametric regimes corresponding to the three different dynamical states, namely, synchronous, chimera, and asynchronous, we calculate the conventional statistical measure strength of incoherence (SI)[18,32] as

06 October 2025 08:30:41

Published under an exclusive license by AIP Publishing

follows:

$$\mathrm{SI} = 1 - \frac{1}{n}\sum_{l=1}^{n} s_l, \qquad s_l = H(d - \sigma(l)), \tag{4}$$

where $H(\cdot)$ is the Heaviside step function, $d = 0.5$ is the threshold, $n = 5$ is the number of bins with length $b = N/n = 20$ of which all oscillators are divided, chosen analogously to,[18] and $\sigma(l)$ is the local standard deviation measured for each bin as

$$\sigma(l) = \left\langle \sqrt{\frac{1}{b}\sum_{i=1+(l-1)b}^{lb} (\Delta\varphi_i - \langle\Delta\varphi\rangle)^2} \right\rangle_t, \tag{5}$$

where $\Delta\varphi_i$ is the difference between φ_i and the closest next φ_j ($j = i+1, \ldots, N, 1, \ldots, i-1$), which is coupled to φ_i according to C^1, $\langle\cdot\rangle_t$ is the average over time, and $\langle\Delta\varphi\rangle$ is the mean value of all $\Delta\varphi_i$,

$$\langle\Delta\varphi\rangle = \frac{1}{N}\sum_{i=1}^{N} \Delta\varphi_i. \tag{6}$$

Then, we define the regime as follows: SI ≤ 0.05 is an asynchronous regime, SI ≥ 0.95 is a synchronous one, and $0.05 <$ SI < 0.95 is a chimera state.

III. RESULTS

Now, to explore the collective behaviors, we consider two different types of network topologies, namely, nonlocal and small-world networks.

A. Nonlocal topology

First, we investigate the behavior of the network of Kuramoto phase oscillators with a nonlocal topology. Previously, such a network without adaptation ($\rho_1 = \rho_2 = 0$) has been investigated in detail in Ref. 18. The authors have shown the presence of a chimera state in a Kuramoto network with higher-order interactions. We investigate the different synchronization regions in Fig. 1(a) by simultaneously varying the coupling strengths L_1 and L_2. To distinguish different regimes, we calculate the conventional statistical measure strength of incoherence (SI) [Eq. (4)]. White, black, and orange regions correspond to a synchronous state (SI ≥ 0.95), an asynchronous state (SI ≤ 0.05), and a chimera state ($0.05 <$ SI < 0.95).

As one can see, all three regimes can be easily separated from each other. The synchronous regime in Fig. 1(a) is observed in the bottom-right triangle with the border line $L_2 \leq 1.2L_1$. Thus, it requires the presence of the first-order couplings, and the strength of the second-order couplings cannot exceed $1.2L_1$. The asynchronous regime is observed on the opposite side in the top left triangle bounded by line $L_2 \geq 2.85L_1$ and requires the presence of the second-order couplings. Between the lines, there is an orange area of a chimera state.

Next, we investigate how the adaptation influences the network's dynamics. Figure 1(b) illustrates the same map as in Fig. 1(a) but with ($\rho_1 = \rho_2 = 0.01$). As one can see, the most part

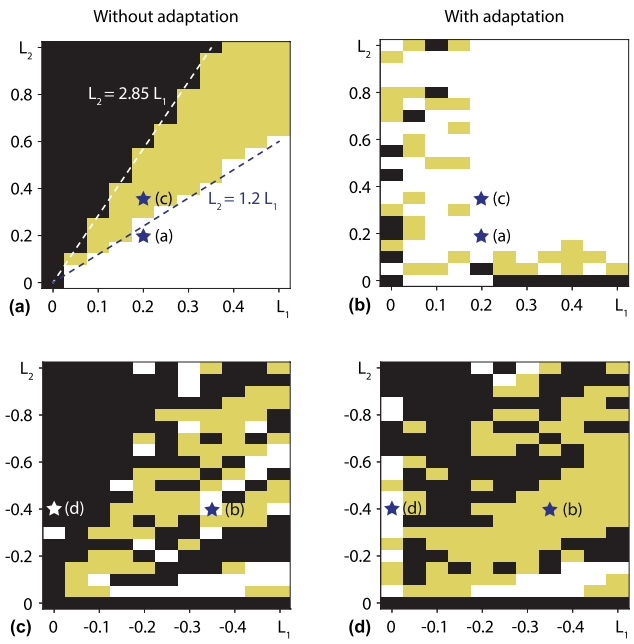

FIG. 1. Maps of characteristic regimes established in the network of coupled Kuramoto oscillators depending on the pairwise coupling strength L_1 and non-pairwise coupling strength L_2 for the nonlocal topology of couplings for (a) and (b) positive and (c) and (d) negative couplings and in the (a) and (c) absence ($\rho_1 = \rho_2 = 0$) and (b) and (d) presence ($\rho_1 = \rho_2 = 0.01$) of the adaptation. Here, white, black, and orange regions represent the regions of synchronous, asynchronous, and chimera states, respectively. The stars indicate the parameters for the time series in Fig. 2.

of it corresponds to the synchronous regime. The asynchronous state is observed mostly for $L_2 = 0, L_1 \in [0.25, 0.5]$, and $L_1 = 0, L_2 \in [0, 0.25]$. The chimera area corresponds to small values of both first and second order coupling strengths.

We should note that the synchronous regime for a system without adaptation always corresponds to one-cluster synchronization, while in the presence of adaptation, we observe antiphase two-cluster synchronization for a wide range of parameters. Figure 2(a) illustrates this effect when adaptation induces antiphase two-cluster synchronization from one-cluster synchronization.

All previous results were obtained using only positive couplings: $L_1 > 0, L_2 > 0$. Then, we investigate the network with only negative couplings. As one can see in Fig. 1(c), the most typical regime for such a case without adaptation is an asynchronous one. Remarkably, without second-order couplings, only the asynchronous regime is observed. However, if the second-order strength is low ($-0.15 \leq L_2 < 0$), for $-0.5 \leq L_1 \leq -0.15$, we can observe a synchronous regime. Turning on the adaptation leads inducing chimera state for a wide range of coupling strengths [Fig. 1(d)]. Also, for $L_1 = 0$ and $-0.6 \leq L_2 \leq -0.05$, an asynchronous regime is turned to a synchronous one.

As a result, adaptation in the Kuramoto network with nonlocal topology can lead to changing a regime. For example, we can induce a chimera state from a two-cluster synchronization regime

06 October 2025 08:30:41

Published under an exclusive license by AIP Publishing

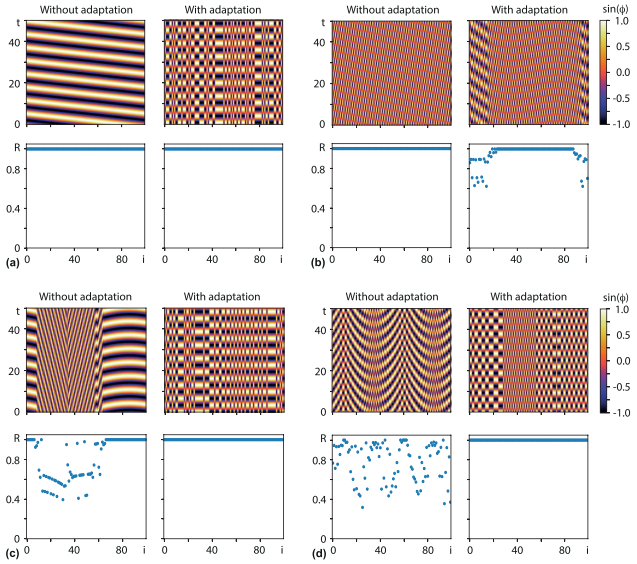

FIG. 2. Spatiotemporal diagrams (top) and local order parameter R_i (bottom) for all phase oscillators of the Kuramoto network illustrating switching between the regimes under the influence of coupling adaptation for the case of nonlocal topology: (a) a transition from the regime of full synchronization with a running phase to the regimes of antiphase synchronization with two clusters at $L_1 = L_2 = 0.2$; (b) a transition from antiphase synchronization to the chimera at $L_1 = -0.35, L_2 = -0.4$; (c) a transition from the chimera state to the regime of antiphase synchronization with two clusters at $L_1 = 0.2, L_2 = 0.35$; and (d) a transition from the asynchronous state to the regime of antiphase synchronization with two clusters at $L_1 = 0, L_2 = -0.4$.

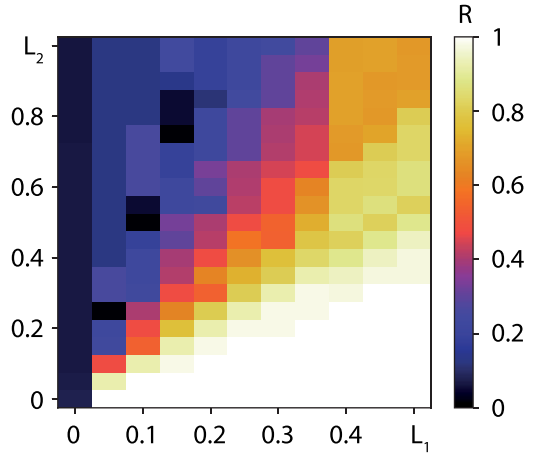

FIG. 3. Two-parameter diagram of the global order parameter of a network of Kuramoto phase oscillators depending on the coupling strengths L_1 and L_2.

[Fig. 2(b)], or oppositely suppress a chimera and induce antiphase two-cluster synchronization [Fig. 2(c)]. Also, it can synchronize the asynchronous state into two antiphase clusters [Fig. 2(d)].

The asymmetry in the effect of adaptation for positive and negative couplings can be attributed to the different roles of attractive and repulsive interactions. Adaptive strengthening of positive couplings favors global synchronization, while adaptive strengthening of repulsive couplings leads to both synchronization and desynchronization, facilitating the emergence of chimera states.

Although the qualitative structure of the phase diagrams is robust to different initial phase conditions, the exact boundaries between dynamical regimes may vary slightly due to multistability.

B. Small-world topology

Then, we investigate another type of network topology, a small-world one, which is characterized by the presence of both local and nonlocal couplings. First, we simulate the network without adaptation. Figure 3 illustrates the dependence of the global order parameter R on the coupling strengths of the first L_1 and the second L_2 orders. As one can see, the maximal $R = 1$ is achieved for maximal $L_1 = 1$ and minimal $L_2 = 0$. The minimal $R = 0.1$, corresponding to the absence of synchronization, is obtained for $L_1 = 0$ and does not depend on L_2. Increasing the first-order couplings and decreasing the second one leads to increasing the global order parameter, and the opposite behavior leads to decreasing R.

Let us consider the case when $L_1 = L_2 = 0.01$ and analyze how adaptation of the couplings of different orders changes the dynamics. Figure 4(a) illustrates an example of time-space dependencies when we adapt only the first-order couplings ($\rho_1 = 0.01$, $\rho_2 = 0$). The vertical line at $T_a = 40$ corresponds to the time moment of starting the adaptation process. As one can see, adaptation of only the first-order couplings leads to one-cluster synchronization. If we adapt only the second-order ones ($\rho_1 = 0$, $\rho_2 = 0.01$), the oscillators form two antiphase clusters [Fig. 4(b)]. In case of adapting both first- and second-order couplings ($\rho_1 = 0.01$, $\rho_2 = 0.01$), we also observe formation of two antiphase clusters but in less time [Fig. 4(c)].

Because the number of oscillators in each synchronous cluster can differ, we investigate the dependence of the cluster's sizes N_1 and N_2 on the adaptation strengths ρ_1 and ρ_2 for $L_1 = L_2 = 0.01$. As one can see in Fig. 5, smaller ρ_2 and larger ρ_1 result in larger N_1 [Fig. 5(a)] and smaller N_2 [Fig. 5(b)] and vice versa. The sum $N_{all} = N_1 + N_2 = 100$ is constant for any adaptation strengths [Fig. 5(c)]. As a result, the global order parameter R is fully correlated with the size of the biggest cluster N_1 [Fig. 5(d)].

We conduct the same investigation for negative couplings ($L_1 = -0.01$, $L_2 = -0.01$). In Fig. 6, one can see that not all oscillators belong to any synchronous cluster ($N_{all} \in [26, 46]$), and the clusters' sizes change within similar ranges ($N_1 \in [11, 22]$, $N_2 \in [11, 25]$) depending on ρ_1 and ρ_2. The number of synchronous oscillators is maximal for $\rho_1 = 0.01$ and $\rho_2 = 0.07$ and 0.08. Increasing ρ_1 and ρ_2 decreases the number of synchronous oscillators and global order parameter [Fig. 6(d)].

Next, we analyze the whole range of positive and negative couplings with and without adaptation. Figure 7(a) illustrates the map of the regimes established in a small-world network depending on the positive coupling strengths L_1 and L_2 without adaptation. As one can see, the asynchronous regime (black area) is observed for any second-order coupling strength L_2 for $L_1 = 0$, and for $L_1 > 0$,

06 October 2025 08:30:41

Published under an exclusive license by AIP Publishing

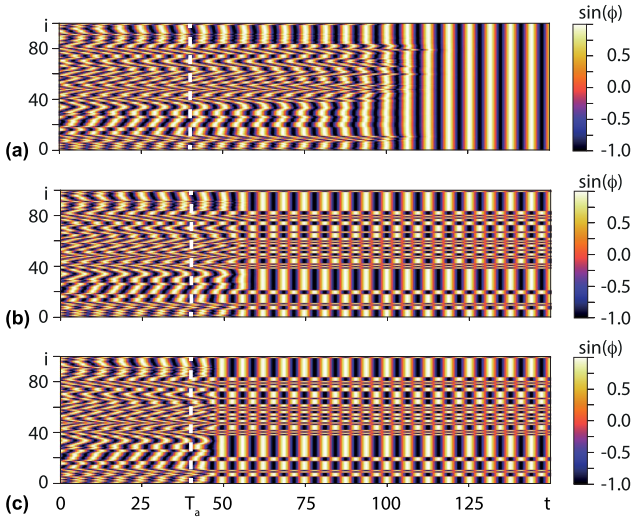

FIG. 4. Time-space dependences of the dynamics of all Kuramoto phase oscillators for $L_1 = L_2 = 0.01$ with adaptation of couplings of (a) only the first order for $\rho_1 = 0.01$, $\rho_2 = 0$; (b) only the second order for $\rho_1 = 0$, $\rho_2 = 0.01$; and (c) the first and second order $\rho_1 = \rho_2 = 0.01$. A vertical white dashed line corresponds to the time moment $T_a = 40$ when the adaptation process starts.

L_2 should be larger than $0.05 + 3.15L_1$. The synchronous regime is established for $L_1 \in (0, 0.5]$ and $L_2 \leq L_1$ and lies in the bottom-right corner. Both boundaries are similar to the nonlocal topology. All other values correspond to the chimera state of partial synchronization. Comparing with Fig. 1(a), we conclude that the parameter

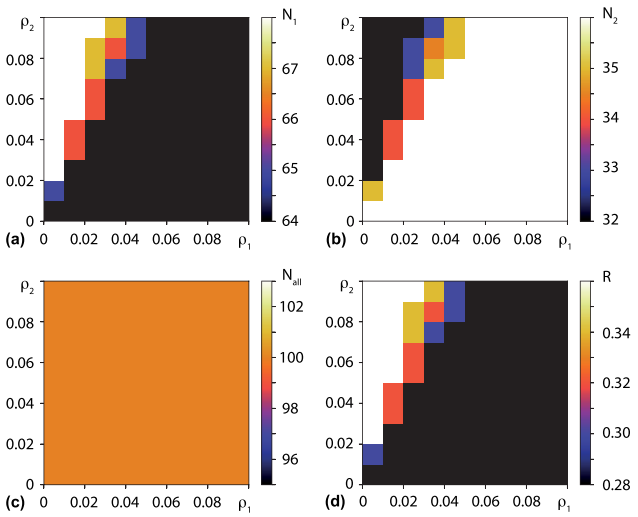

FIG. 5. Two-parametric dependencies on the first- and second-order adaptation strengths ρ_1 and ρ_2 of (a) and (b) the number of oscillators belonging to (a) the first, (b) the second, and (c) both synchronous clusters, and (d) the global order parameter. Here, $L_1 = 0.01$ and $L_2 = 0.01$.

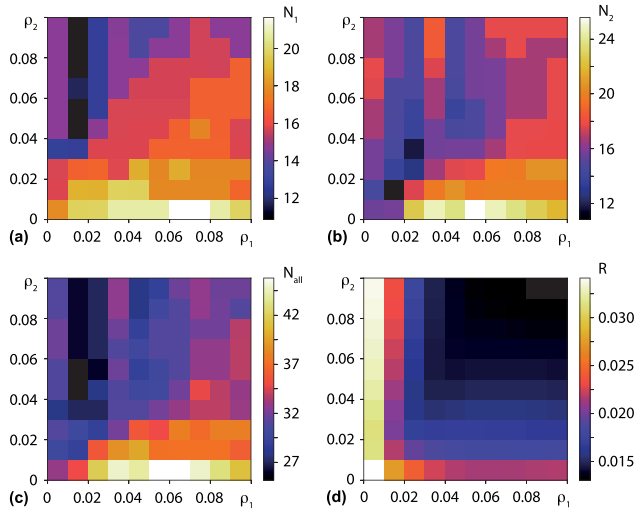

FIG. 6. Two-parametric dependencies of (a)–(c) the number of oscillators belonging to (a) the first, (b) the second, and (c) both synchronous clusters, and (d) the global order parameter on adaptation strengths of first- and second-order ρ_1 and ρ_1. Here, $L_1 = -0.01$ and $L_2 = -0.01$.

region corresponding to chimera states is larger for the small-world topology than for the nonlocal one, while synchronous and asynchronous areas are smaller.

Adaptation of the positive couplings in such a network [Fig. 7(b)] leads to almost disappearance of an asynchronous regime, which is observed only for $L_2 = 0$ and $L_1 \in [0.25, 0.5]$. The chimera state is observed for either low first- or second-order couplings, while the initial chimera area is transformed to a synchronous one.

In case all couplings are negative [Fig. 7(c)], only asynchronous and a chimera states can be observed, and the latter is established only for $0 > L_2 \geq 1.5L_1$. The adaptation of negative couplings in a small-world network of Kuramoto phase oscillators expands the area of the chimera state and also allows establishing a synchronous regime for $L_1 = 0$ and $L_2 > 0$. One can see that for $L_2 = 0$, whether adaptation is present or not, only the asynchronous regime is observed, and this is independent of L_1.

We should note that in the case of small-world topology, randomness plays an important role in forming a particular coupling matrix. It can be crucial, for example, in reservoir computing where the specific topology of the reservoir layer network strongly influences the accuracy.[33–38] To investigate the influence of the particular topology on the system's dynamics, we randomly generate five different coupling matrices using a Watts–Strogatz algorithm with the same parameters ($k = 5, p = 0.3$) and simulate the network of Kuramoto phase oscillators [Eqs. (1)–(3)] using each of them started with the same initial conditions. Then, we calculate the strength of incoherence [Eq. (4)], average it over all five topologies and define the regime.

The obtained maps are shown in Figs. 7(e)–7(h). As one can see, the area of a chimera state has become larger for all considered cases. The boundaries of synchronous and asynchronous regimes for the case of positive couplings without adaptation [Fig. 7(e)]

06 October 2025 08:30:41

Published under an exclusive license by AIP Publishing

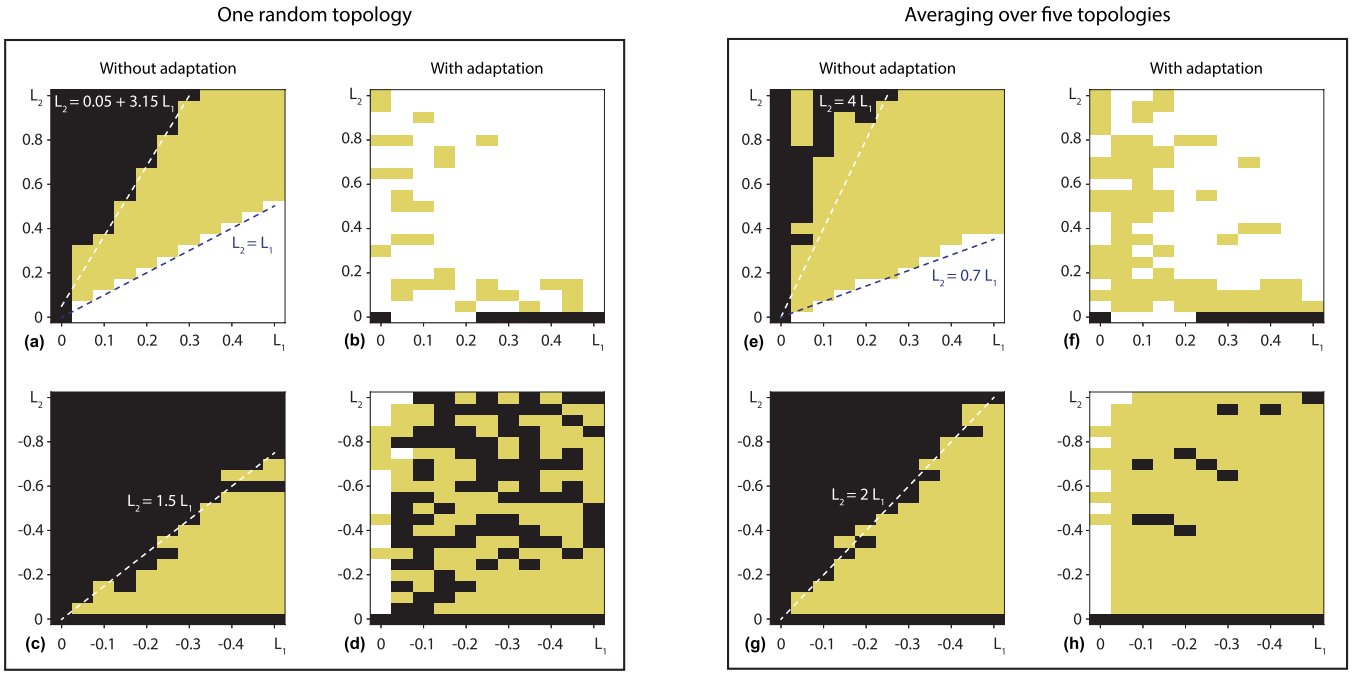

FIG. 7. Maps of characteristic regimes established in the network of coupled Kuramoto oscillators depending on the coupling strengths of the first L_1 and second L_2 orders for (a)–(d) a random small-world topology of couplings and (e)–(h) averaged over five topologies for (a), (b), (e), and (f) positive and (c), (d), (g), and (h) negative couplings and in the (b), (d), (f), and (h) presence ($\rho_1 = \rho_2 = 0.01$) and (a), (c), (e), and (g) absence ($\rho_1 = \rho_2 = 0$) of the adaptations. Here, white, black, and orange regions represent the synchronous, asynchronous, and chimera states, respectively.

have changed to $L_2 = 0.7L_1$ and $L_2 = 4L_1$, respectively, reducing the corresponding areas. When adaptation is active, the area of an asynchronous regime has not changed over averaging, but the chimera state is now observed for almost any parameters in the following ranges: $0 < L_2 < 0.2$ for any L_1 and $L_1 < 0.2$ for $L_2 > 0$.

In the case of negative couplings [Fig. 7(g)], similar to (c), only asynchronous and chimera states can be observed, but the boundary line is changed to $L_2 = 2L_1$, increasing the area of the chimera state. In the presence of adaptation, the asynchronous regime almost completely disappears, so the area of $L_1 > 0$ and $L_2 > 0$ corresponds to chimera, while $L_2 = 0$ is the asynchronous state and $L_1 = 0$, $L_2 > 0$ is the synchronous one.

IV. CONCLUSION

In this work, we investigated the dynamics of a network of Kuramoto phase oscillators with adaptation of first- and second-order couplings in two different topologies: nonlocal and small-world. The primary focus was on studying the influence of coupling adaptation on the emergence and transition between synchronization regimes, including the chimera state.

We found that adaptation of the couplings plays a crucial role in establishing the regime in the network. It can lead to inducing a chimera state from the two antiphase clusters, or oppositely suppress a chimera and induce the state of antiphase two-cluster synchronization. It can also lead to synchronization of the asynchronous regime and vice versa. These effects are observed for both investigated topologies. For nonlocal topology depending on the coupling strength of the first and second order, any of three regimes can be observed with and without adaptation in a wide range of the coupling strengths. For small-world topology in the case of using only negative couplings, only two regimes exist without adaptation, and the adaptation induces a synchronous regime in a small range of the parameters. For the case of using only positive couplings for small-world topology with adaptation of the couplings, mostly two regimes (synchronous and chimera) exist, while the asynchronous one is observed for only a few values of the coupling strengths.

We investigated the influence of the particular small-world topology realization by averaging the results over five random topologies with the same parameters and initial conditions. It was found that such averaging leads to an increase in the area of the parameters corresponding to the chimera state. Particularly, adaptation of negative couplings on average leads to chimera states, while synchronous and asynchronous regimes exist only in the absence of either first- or second-order couplings.

The obtained results open new possibilities for controlling the dynamics of complex networks in various applications, including neuroscience and complex systems theory.

Future work may explore mixed-sign couplings (e.g., $L_1 > 0$, $L_2 < 0$ or $L_1 < 0$, $L_2 > 0$), which could lead to novel synchronization patterns and further enrich the control of chimera states via adaptive higher-order interactions.

06 October 2025 08:30:41

Published under an exclusive license by AIP Publishing

ACKNOWLEDGMENTS

This work was supported by the Russian Science Foundation (Grant No. 23-71-30010).

AUTHOR DECLARATIONS

Conflict of Interest

The authors have no conflicts to disclose.

Author Contributions

Andrey V. Andreev: Conceptualization (equal); Investigation (equal); Methodology (equal); Software (equal); Supervision (equal); Validation (equal); Visualization (equal); Writing – original draft (equal). **Artem A. Badarin:** Conceptualization (equal); Formal analysis (equal); Investigation (equal); Software (equal); Validation (equal); Writing – original draft (equal). **Dibakar Ghosh:** Conceptualization (equal); Methodology (equal); Writing – review & editing (equal). **Elena N. Pitsik:** Formal analysis (equal); Methodology (equal); Writing – original draft (equal). **Alexander E. Hramov:** Conceptualization (equal); Formal analysis (equal); Funding acquisition (equal); Methodology (equal); Supervision (equal); Writing – review & editing (equal).

DATA AVAILABILITY

The data that support the findings of this study are available from the corresponding author upon reasonable request.

REFERENCES

[1] A. Pikovsky, M. Rosenblum, and J. Kurths, *Synchronization* (Cambridge University Press, 2001), Vol. 12.
[2] P. K. Pal, M. S. Anwar, M. Perc, and D. Ghosh, "Global synchronization in generalized multilayer higher-order networks," Phys. Rev. Res. **6**, 033003 (2024).
[3] S. Boccaletti, J. Kurths, G. Osipov, D. Valladares, and C. Zhou, "The synchronization of chaotic systems," Phys. Rep. **366**, 1–101 (2002).
[4] A. V. Andreev, V. A. Maksimenko, A. N. Pisarchik, and A. E. Hramov, "Synchronization of interacted spiking neuronal networks with inhibitory coupling," Chaos, Solitons Fractals **146**, 110812 (2021).
[5] A. A. Koronovskii, O. I. Moskalenko, A. A. Pivovarov, V. A. Khanadeev, A. E. Hramov, and A. N. Pisarchik, "Jump intermittency as a second type of transition to and from generalized synchronization," Phys. Rev. E **102**, 012205 (2020).
[6] J. A. Acebrón, L. L. Bonilla, C. J. Pérez Vicente, F. Ritort, and R. Spigler, "The Kuramoto model: A simple paradigm for synchronization phenomena," Rev. Mod. Phys. **77**, 137–185 (2005).
[7] F. A. Rodrigues, T. K. D. Peron, P. Ji, and J. Kurths, "The Kuramoto model in complex networks," Phys. Rep. **610**, 1–98 (2016).
[8] N. Frolov and A. Hramov, "Extreme synchronization events in a Kuramoto model: The interplay between resource constraints and explosive transitions," Chaos **31**, 063103 (2021).
[9] N. Frolov and A. Hramov, "Self-organized bistability on scale-free networks," Phys. Rev. E **106**, 044301 (2022).
[10] M. I. Bolotov, V. O. Munyayev, L. A. Smirnov, G. V. Osipov, and I. Belykh, "Breathing and switching cyclops states in Kuramoto networks with higher-mode coupling," Phys. Rev. E **109**, 054202 (2024).
[11] P. K. Pal, N. Frolov, S. Rakshit, A. E. Hramov, and D. Ghosh, "Explosive synchronization in generalized multiplex network with competitive and cooperative interlayer interactions," Chaos **35**, 071102 (2025).
[12] C. Bick, E. Gross, H. A. Harrington, and M. T. Schaub, "What are higher-order networks?" SIAM Rev. **65**, 686–731 (2023).
[13] R. Lambiotte, M. Rosvall, and I. Scholtes, "From networks to optimal higher-order models of complex systems," Nat. Phys. **15**, 313–320 (2019).
[14] S. Boccaletti, P. De Lellis, C. Del Genio, K. Alfaro-Bittner, R. Criado, S. Jalan, and M. Romance, "The structure and dynamics of networks with higher order interactions," Phys. Rep. **1018**, 1–64 (2023).
[15] S. Majhi, M. Perc, and D. Ghosh, "Dynamics on higher-order networks: A review," J. R. Soc. Interface **19**, 20220043 (2022).
[16] F. Battiston, E. Amico, A. Barrat, G. Bianconi, G. Ferraz de Arruda, B. Franceschiello, I. Iacopini, S. Kéfi, V. Latora, Y. Moreno *et al.*, "The physics of higher-order interactions in complex systems," Nat. Phys. **17**, 1093–1098 (2021).
[17] P. Jaros, S. Ghosh, D. Dudkowski, S. K. Dana, and T. Kapitaniak, "Higher-order interactions in Kuramoto oscillators with inertia," Phys. Rev. E **108**, 024215 (2023).
[18] S. Kundu and D. Ghosh, "Higher-order interactions promote chimera states," Phys. Rev. E **105**, L042202 (2022).
[19] R. Ghosh, U. K. Verma, S. Jalan, and M. D. Shrimali, "First-order transition to oscillation death in coupled oscillators with higher-order interactions," Phys. Rev. E **108**, 044207 (2023).
[20] A. A. Emelianova and V. I. Nekorkin, "Synchronization and chaos in adaptive Kuramoto networks with higher-order interactions: A review," Regul. Chaotic Dyn. **30**, 57–75 (2025).
[21] R. Ghosh, U. K. Verma, S. Jalan, and M. D. Shrimali, "Chimeric states induced by higher-order interactions in coupled prey–predator systems," Chaos **34**, 061101 (2024).
[22] M. J. Panaggio and D. M. Abrams, "Chimera states: Coexistence of coherence and incoherence in networks of coupled oscillators," Nonlinearity **28**, R67 (2015).
[23] S. Majhi, B. K. Bera, D. Ghosh, and M. Perc, "Chimera states in neuronal networks: A review," Phys. Life Rev. **28**, 100–121 (2019).
[24] N. Frolov, V. Maksimenko, S. Majhi, S. Rakshit, D. Ghosh, and A. Hramov, "Chimera-like behavior in a heterogeneous Kuramoto model: The interplay between attractive and repulsive coupling," Chaos **30**, 081102 (2020).
[25] A. Andreev, N. Frolov, A. Pisarchik, and A. Hramov, "Chimera state in complex networks of bistable Hodgkin-Huxley neurons," Phys. Rev. E **100**, 022224 (2019).
[26] N. S. Frolov, V. A. Maksimenko, V. V. Makarov, D. V. Kirsanov, A. E. Hramov, and J. Kurths, "Macroscopic chimeralike behavior in a multiplex network," Phys. Rev. E **98**, 022320 (2018).
[27] G. Bianconi, *Higher-Order Networks* (Cambridge University Press, 2021).
[28] I. Iacopini, G. Petri, A. Barrat, and V. Latora, "Simplicial models of social contagion," Nat. Commun. **10**, 2485 (2019).
[29] R. Berner, T. Gross, C. Kuehn, J. Kurths, and S. Yanchuk, "Adaptive dynamical networks," Phys. Rep. **1031**, 1–59 (2023).
[30] G. E. Ha and E. Cheong, "Spike frequency adaptation in neurons of the central nervous system," Exp. Neurobiol. **26**, 179 (2017).
[31] D. J. Watts and S. H. Strogatz, "Collective dynamics of "small-world" networks," Nature **393**, 440–442 (1998).
[32] R. Gopal, V. Chandrasekar, A. Venkatesan, and M. Lakshmanan, "Observation and characterization of chimera states in coupled dynamical systems with nonlocal coupling," Phys. Rev. E **89**, 052914 (2014).
[33] A. E. Hramov, N. Kulagin, A. N. Pisarchik, and A. V. Andreev, "Strong and weak prediction of stochastic dynamics using reservoir computing," Chaos **35**, 033140 (2025).
[34] A. Griffith, A. Pomerance, and D. J. Gauthier, "Forecasting chaotic systems with very low connectivity reservoir computers," Chaos **29**, 123108 (2019).
[35] A. Badarin, A. Andreev, V. Klinshov, V. Antipov, and A. E. Hramov, "Hidden data recovery using reservoir computing: Adaptive network model and experimental brain signals," Chaos **34**, 103121 (2024).
[36] M. Dale, S. O'Keefe, A. Sebald, S. Stepney, and M. A. Trefzer, "Reservoir computing quality: Connectivity and topology," Nat. Comput. **20**, 205–216 (2021).
[37] A. V. Andreev, A. N. Pisarchik, N. Kulagin, R. Jaimes-Reátegui, G. Huerta-Cuellar, A. A. Badarin, and A. E. Hramov, "Stochastic cloning of dynamical systems with hidden variables," Phys. Rev. E **112**, 015303 (2025).
[38] Y. Kawai, J. Park, and M. Asada, "A small-world topology enhances the echo state property and signal propagation in reservoir computing," Neural Netw. **112**, 15–23 (2019).

06 October 2025 08:30:41

Published under an exclusive license by AIP Publishing